

Biophysical Mechanism of the SAHA Inhibition of Zn²⁺-Histone Deacetylase-Like Protein (FB188 HDAH) Assessed via Crystal Structure Analysis

Cynthia Raquel Trejo-Muñoz¹, Ricardo Vázquez-Ramírez², Luis Mendoza², Carlos Kubli-Garfias^{2*}

¹Escuela Superior de Medicina, Instituto Politécnico Nacional, Ciudad de México, México

²Instituto de Investigaciones Biomédicas, Universidad Nacional Autónoma de México, Ciudad de México, México

Email: *kubli@unam.mx

How to cite this paper: Trejo-Muñoz, C.R., Vázquez-Ramírez, R., Mendoza, L. and Kubli-Garfias, C. (2018) Biophysical Mechanism of the SAHA Inhibition of Zn²⁺-Histone Deacetylase-Like Protein (FB188 HDAH) Assessed via Crystal Structure Analysis. *Computational Molecular Bioscience*, 8, 91-114.

<https://doi.org/10.4236/cmb.2018.82005>

Received: May 19, 2018

Accepted: June 25, 2018

Published: June 28, 2018

Copyright © 2018 by authors and Scientific Research Publishing Inc. This work is licensed under the Creative Commons Attribution International License (CC BY 4.0).

<http://creativecommons.org/licenses/by/4.0/>



Open Access

Abstract

The zinc-containing enzyme HDAC-like amidohydrolase (FB188 HDAH), identified in the *Bordetella alcaligenes* bacteria, is similar to enzymes that participate in epigenetic mechanisms such as histone modifications. The X-ray crystal structure of FB188 HDAH complexed with the antagonist SAHA (suberoylanilide hydroxamic acid) has been solved (PDB ID: 1ZZ1). Notably, the complex crystallizes as a tetramer in the asymmetric unit cell of the crystal. The crystal yielded a suitable structure to analyze the dynamics of the inhibitory mechanism of SAHA on this histone deacetylase. Applying computational chemistry techniques and quantum mechanics theory, several physicochemical properties were calculated to compare the active site of the enzyme of the four monomers. Significant differences were observed in the areas and volumes of the binding pocket, as well as hydrophobic interactions, dipole moments, atomic charges and electrostatic potential, among other properties. Remarkably, a free-energy curve resulting from the evaluation of the energies of SAHA and the interacting amino acids of the four crystal monomers unveiled the biophysical mechanism of the FB188 HDAH inhibition exerted by SAHA to a greater extent. The biophysical mechanism of SAHA inhibition on FB188 deacetylase was clearly observed as a dynamic process. It is possible to define the physicochemical dynamics of the molecular complex by the application of computational chemistry techniques and quantum mechanics theory by studying the crystal structures of the interacting molecules.

Keywords

SAHA, Deacetylase, FB188 HDAH, Free-Energy, Crystal-Analysis

1. Introduction

Three classes of histone deacetylases (HDACs) have been found using phylogenetic analysis of all HDAC-related proteins. These have been divided into three groups, namely: Class 1, class 2, and a third class related to the human HDAC11 gene; the third group has been classified as “class 4” since the term “class 3” was previously reserved for unrelated sirtuin deacetylases [1]. According to the sequence similarity classes 1 and 2 (also named I and II), HDACs share significant homology in their catalytic sites and feature a coordinated zinc atom. Class 3 (also termed “III”) is a well-conserved family of Sir2-nicotinamide adenine dinucleotide-(NAD) dependent deacetylases [2]. Class 1 and 2 HDACs are zinc metalloenzymes that act similarly to histone acetyltransferases (HAT) at the lysine residues of the histone cores that are complexed with DNA to form the nucleosomes. HDAC and HAT deacetylate and acetylate, respectively, the NH_3^+ group of lysine that modulates gene expression to some extent. HDAC, in particular, have been associated with gene silencing; however, the opposite has also been proposed: HDACs may also be able to activate the gene [3].

Histone acetylation is a dynamic, reversible process that allows chromatin remodeling and directly influences gene expression. However, the cellular function of HDACs is not restricted to chromatin remodeling. There is evidence that HDACs participate in acetylation of non-histone proteins [4]. Some epigenetic mechanisms, such as histone modifications, are exerted by HDACs along with HATs. Both types of enzymes determine a pattern of histone deacetylation-acetylation that is involved in the regulation of gene expression [2]. Some pathological processes may occur as a consequence of dysfunctional histone acetylation processes. The diseases associated with histone acetylation-deacetylation failure include cancer and abnormal proliferative process [5], neurodegenerative and mental disorders such as Alzheimer disease [6], schizophrenia [7] and cardiovascular diseases such as atherosclerosis and restenosis [8]. The enzymatic activity of HDACs seems to increase in the aforementioned diseases. In fact, HDACs inhibitors have been clinically proven successful in many pathological entities.

The molecular mechanism of HDACs inhibitors has been elucidated, describing the role of the residues and the zinc-ion in the binding site as well as structural details of a histone deacetylase-like protein obtained from *Aquifex aeolicus*, an anaerobic bacterium that is inhibited by trichostatin A (TSA) and suberoylanilide hydroxamic acid (SAHA) [9]. Likewise, the crystal structure and analysis of HDAC7 [10], HDAC8 [11] and HDAC2 [12], among other HDAC-like proteins, have provided important insight into the mechanism of action of some HDAC inhibitors [13]. Interestingly, a bacterial HDAC-like amidohydrolase has been cloned from *Bordetella alcaligenes*. The sequence database analysis of FB188 HDAH confirms that this amidohydrolase belongs to the family of HDACs and bears a Zn^{2+} ion in its catalytic core. This enzyme exhibits significant activity in standard HDAC assays and is also inhibited by TSA and SAHA

[14]. The crystal structure of FB188 HDAH has been solved (PDB ID: 1ZZ) and used as a model for the catalytic core of class 2 HDACs due to their significant homology [15].

Notably, the HDAC-like protein FB188 complexed with SAHA (PDB ID: 1ZZ1) crystallizes as a tetramer in the asymmetric unit cell of the crystal [15]. The four monomers appear suitable to analyze the atomic interactions of the enzyme-inhibitor complex and to calculate the free energy of the catalytic process in a dynamic way. Our hypothesis assumes that the SAHA-FB188 tetramer in the asymmetric unit cell of the crystal (**Figure 1**) can be useful to elucidate the dynamics of the enzyme-inhibitor biophysics through the measurement of the interatomic binding process. Each monomer of the crystal structure represents a glimpse of a continuum process.

2. Methods

2.1. Crystal

The 1.57 Å crystal structure of the histone deacetylase-like enzyme from the *Bordetella alcaligenes* strain FB188 (FB188 HDAH) with the PDB ID: 1ZZ1 was downloaded from the Protein Data Bank (PDB) [16]. The enzyme is complexed with the SAHA ligand, including a coordinated Zn^{2+} metal ion in the binding pocket, and crystallizes as a tetramer in the asymmetrical unit cell of the crystal. In the PDB crystal, four protein monomers named A, B, C and D, were separated into mA, mB, mC and mD nomenclature for the entire study.

The four molecules of SAHA were extracted from the four protein monomers. After that, each SAHA molecule was analyzed according to three structural regions: the anilide group (an amide-phenyl group); the suberoyl middle group derived from octanedioic acid, and the hydroxamic acid group. Interestingly, the

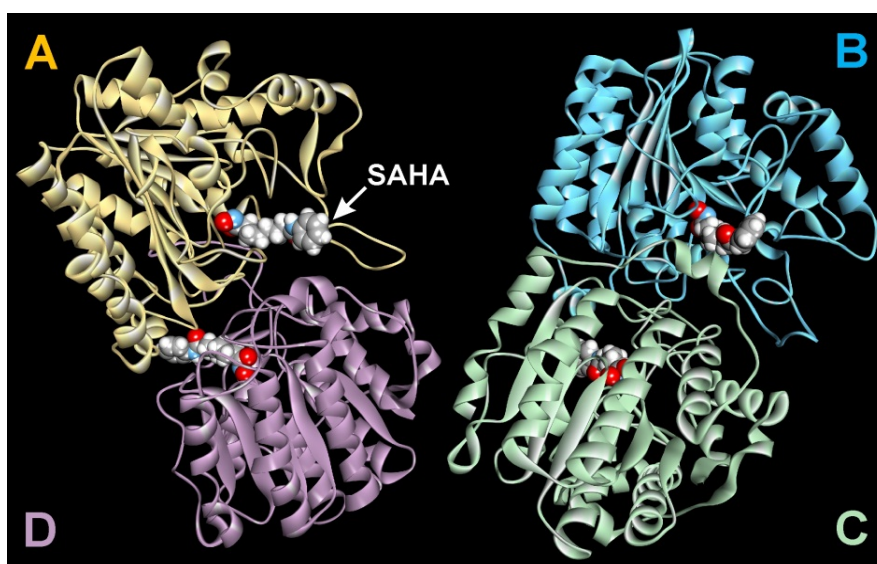


Figure 1. The 1.57 Å crystal structure of the FB188 HDAH enzyme (PDB ID: 1ZZ1), shows the asymmetric unit arrangement with four monomers (A, B, C and D) in complex with SAHA inhibitor in van der Waals surface.

covalent bond between the anilide moiety and the suberoyl acid forms a peptide-like bond. The differences among the four SAHA structures were assessed by measuring the torsion angles in the suberoyl chain and calculating the root-mean-square deviation (RMSD) of overlapping pairs of SAHA monomers using the VMD program [17]. The SAHA molecule in mB had outlier characteristics, with different conformation in the anilide and suberoyl regions. To assess the reliability and confident conformation of the SAHA molecules, the B-factor (thermal-factor) was obtained directly from the 1ZZ1-PDB file to compare the range of atomic motion among the monomers. Whenever necessary, torsion angles and other molecular structure parameters were changed slightly to adjust the crystal structure before applying any calculation. In addition, the catalytic site was identified using the Ligand Explorer software [18]. The binding core was offset by 4 Å, including 11 residues that surround SAHA and Zn²⁺ at this distance.

From this framework for the SAHA-histone complex, hydrophobic interactions, hydrogen bonds and Zn²⁺ metal coordination were studied. The catalytic site of each of the four monomers was analyzed individually. The following 11 residues that form the first core for each monomer were analyzed: Leu21, Ile100, His142, His143, Phe152, Asp180, His182, Phe208, Asp268, and Tyr312 (from a single monomer), and Phe341 (the 11th residue, which participates from the adjacent asymmetric monomer). Zn²⁺ ion coordination was part of the catalytic site and was also included. All these elements were selected to define the biophysical mechanism of SAHA-antagonism to the FB188 HDAH enzyme.

2.2. Binding Interaction Assessment of SAHA in the Enzyme Catalytic Pocket

The binding mode for each monomer was evaluated by calculating the free energy of SAHA and the binding core of amino acids, comprising three types of interaction, namely hydrophobic interactions, hydrogen bonds and Zn²⁺ ion coordination interactions. The crystal was used to measure the dihedral angles of SAHA-interacting atoms and those of side-chains of the involved amino acids, as well as interacting distances of SAHA and Zn²⁺ coordination with the residues that form the catalytic site, the number of hydrophobic interactions, hydrogen bonds and metal contacts using Ligand Explorer software [18]. In the case of Asp180 and Asp268, the H-bond energy was calculated by slightly adjusting two of the three interacting H-atoms to obtain the optimal distance and minimum energy value. Likewise, in mB and mC, the χ_2 and χ_1 dihedral angles of Ile100 and Phe341 were slightly rotated to correct abnormal atomic distances with SAHA. The binding pocket volume from each monomer was calculated for comparison with the Detector Cavity Tool of the DeepView/Swiss PDB viewer 4.1.0 [19]. To preserve the atomic arrangement of the crystal in the binding site, only single point calculations were carried out. In this way, dipole moment, atomic charges and electrostatic potentials were calculated. Likewise, the binding Gibbs free energy for each of the four monomers calculated. The Density Func-

tional Theory (DFT) was applied with the ω B97X-D functional at the 6-31G* basis set level. All calculations were performed using Spartan' 14 software [20].

2.3. Atomic Charge Calculations

Atomic charges of SAHA and the residues that form the binding pocket were calculated for each monomer. The variation in atomic charges under the bound and unbound conditions was calculated, and the resulting differences were assessed and plotted.

2.4. Molecular Electrostatic Potential Determination

The surface of the molecular electrostatic potential (MEP) was derived from DFT calculations using the ω B97X-D functional and 6-31G* basis set level of theory. Isodensity surfaces were set to 0.002 a.u., and the property range was -200 to 200 kJ/mol.

2.5. Total Free Energy Assessment

The total free energy of the binding pocket core was assessed separately for each monomer. Three steps were followed to determine the total free energy. The first step individually evaluates the energy of each of the 11 residues (Aa) that form the first core at 4 Å, plus the energy of SAHA. The second step gives the energy of each of the Aa-zinc interactions and uses a similar procedure for SAHA-zinc interactions (SAHA-Zn). The third step determines the total free energy of each of the four monomer complexes. Each step is represented by an equation as follows:

Free energy calculation for each of the seven residues interacting with SAHA

$$\Delta E_{\text{AaSAHA}} = E_{\text{AaSAHA}} - (E_{\text{Aa}} + E_{\text{SAHA}}) \quad (1)$$

where ΔE_{AaSAHA} is the free energy from amino acid-SAHA complex, $E_{\text{Aa/SAHA}}$ is the energy calculated for the amino acid residue-SAHA complex, E_{Aa} is the energy for amino acid residues that interact with ligand, and E_{SAHA} is the single point energy for ligand SAHA.

Free energy calculation of either amino-acid zinc, or SAHA-zinc paired interactions

$$\Delta E_{\text{ZnAa or ZnSAHA}} = E_{\text{Zn/SAHA}} \text{ or } E_{\text{Zn/Aa}} - (E_{\text{Zn}} + E_{\text{SAHA}} \text{ or } E_{\text{Aa}}) \quad (2)$$

where $\Delta E_{\text{ZnAa or ZnSAHA}}$ is the free energy of amino acid residue-Zn²⁺ complex or ligand-Zn²⁺ complex, $E_{\text{Zn/SAHA}}$ or $E_{\text{Zn/Aa}}$ is the energy calculated for the ligand-Zn²⁺ or the amino acid -Zn²⁺ interactions, E_{Zn} is the energy for ion Zn²⁺, E_{SAHA} is the energy for ligand SAHA and, E_{Aa} is the energy for amino acid residues that interact with Zn²⁺.

The total free energy of each complex was obtained as indicated in equation (3).

$$\Delta E_T = \Delta E_{\text{AaSAHA}} + \Delta E_{\text{ZnAa}} + \Delta E_{\text{ZnSAHA}} \quad (3)$$

where ΔE_T is the total free energy for the catalytic site of each monomer, A, B, C

and D.

All molecular energies were assessed using single point calculations, as stated previously. The total free energy value for each monomer was fitted to the SAHA inhibition curve of the enzyme FB188 HDAH reported by Hildmann, *et al.* [14].

3. Results

3.1. SAHA Structure and Electronic Properties

At first glance, the SAHA molecule showed conformational differences among the four monomers, to a lesser extent in monomer B and monomer C.

The conformational differences for SAHA were revealed to some extent by the B-factor taken from the 1ZZ1-PDB data, showing the highest mean value of 20.5 Å² form B compared to mD, mA and mC (14.3, 15.6 and 16.0 Å², respectively). Those differences in B-factor, denotes larger atomic motion and higher flexibility for mB compared with three other SAHA molecules. The anilide group of mB and mC was somewhat opposite to mA and mD. Some torsional angles were quite different in mB and mC, mostly those including atoms from C2 to C10 of the SAHA molecule. The direct measurement of the dihedral angle C8-N2-C9-C10, which includes the phenyl ring of SAHA, was 90° for mB, but for mA, mC and mD were 135°, 138° and 134°, respectively, showing that the ring is able to rotate. **Table 1** shows several torsion angles for the four SAHA molecules; mB was the most variable, followed by mC.

Additionally, in mB, the angles χ_2 (C α -C β -C γ 1-C δ) and χ_1 (N-C α -C β -C γ) of Ile100 and Phe341 showed abnormally short hydrophobic distances to the C6 and C7 atoms of SAHA. Both χ_2 and χ_1 angles were rotated in a one-degree step: χ_2 from 159.83° to 99.83° and χ_1 from 174.70° to 168.70°, in this case, only six degrees were needed to achieve trustworthy structural parameters. Thus, the C δ 1 atom of Ile100 was adjusted to the C6 and C7-SAHA atoms and the C ϵ 1 atom of Phe341 to C7 and C8 SAHA atoms. Consequently, all these atoms were corrected to uphold reliable van der Waals distances.

All mB and mC corrections were a prerequisite to proceeding with physico-chemical and energy calculations. Thus, regardless of the adjusted conformation to mB-SAHA, this molecule showed the highest total energy and the largest HOMO-LUMO gap. **Table 2** shows values for the important electronic and physicochemical properties of the four SAHA conformers.

Because of the significant differences in conformation, the four molecules of SAHA showed marked differences in electrostatic potential and dipole moment vectors. This implies different atomic charge arrangements and different total energy. **Figure 2** shows the structure, atom numbering, dipole moment and electrostatic potential for the four SAHA molecules. Each monomer has been labeled with its respective letter and a different color to facilitate identification.

The superimposition of pairs of the four monomers of SAHA to calculate the RMSD values showed that two pairs of monomers, AC and AD, were markedly similar, with the lowest RMSD score. However, the CD pair showed higher

Table 1. Torsion angles ($^{\circ}$) differences among SAHA molecules in the four monomers.

SAHA	C2-C3-C4-C5	C3-C4-C5-C6	C4-C5-C6-C7	C5-C6-C7-C8	C6-C7-C8-N2	C7-C8-N2-C9	C8-N8-C9-C10
mA	52.64	160.21	-177.83	167.29	-121.36	177.22	135.42
mB	161.75	-101.15	-126.88	-118.01	-134.64	171.55	89.71
mC	80.99	162.43	159.68	117.99	77.31	177.28	138.02
mD	68.29	156.72	168.23	168.88	-117.97	176.84	133.65

*Bold values in mB and mC are significantly different from mA and mD.

Table 2. Electronic and physicochemical properties of the four SAHA molecules.

	Energy* (a.u.)	Dipole (Debye)	Volume (\AA^3)	E_{HOMO} (eV)	E_{LUMO} (eV)
SAHA-B	-880.321846	5.50	281.35	-8.83	1.60
SAHA-A	-880.342772	5.65	281.11	-8.74	1.56
SAHA-C	-880.346274	4.67	281.40	-8.17	1.58
SAHA-D	-880.365679	6.64	280.86	-8.30	1.54

*Energy arranged from the highest to the lowest value.

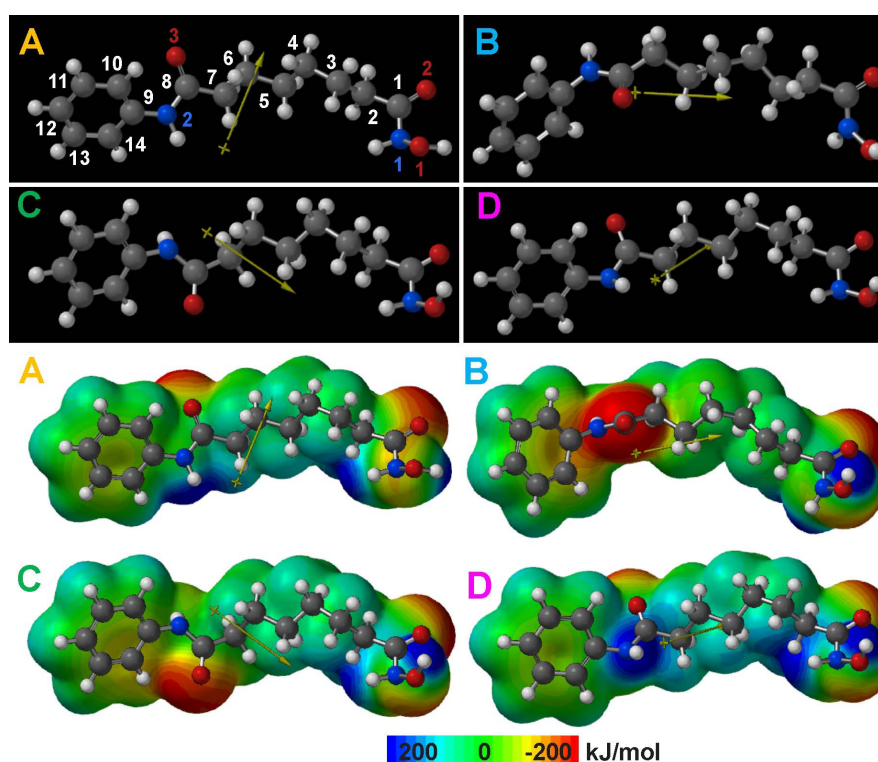


Figure 2. SAHA structures of A, B, C and D monomers from the FB188 HDAH enzyme crystal, on panel A, are showed both atoms numbering and colors of SAHA atoms. Carbons (grey), oxygens (red) and nitrogens (blue). Differences in SAHA conformation are clearly observed, highlighted by the electrostatic potential maps encoded in a van der Waals surface. The carbonyl group of the anilide group shows similar positions in mA and mD, but some differences in the suberoyl hydrophobic chain. The hydroxamic acid group maintains almost the same conformation in all four cases. The dipole moment vector (yellow arrows) points in different directions. Electrostatic potential values were cut-off at 200 (blue) and -200 (red) kJ/mol. Grey, red, blue and white are for C, O, N and H, respectively.

values. Clearly, two of the three pairs where monomer B participates (AB and BD) showed the highest RMSD values. **Table 3** shows all RMSD scores for the six pairs that result from the four monomer combinations.

3.2. Binding Pocket Area and Volume

The binding pocket volume of the FB188 HDAH enzyme showed marked differences among the four cavities where SAHA is bound. To conserve the idea of variability among monomers and logical sequence, the binding pocket volume and SAHA area showed according to the following trend: mB < mD < mC < mA. The SAHA volume, however, remained almost unchanged in the four monomers, showing the following trend mD < mA < mB < mC. **Figure 3** depicts the binding pocket shape and position of the four monomers of the enzyme. The trend values of the binding pocket volume and SAHA physical properties are shown in **Table 4**.

3.3. Overview of the Conformational Variations of SAHA and Binding Pocket Residues

The superimposition of the SAHA-binding pocket cut-off at 4 Å includes the 11 nearest amino acids and the zinc ion, showing that the hydroxamic acid region of SAHA is an important H-bond network concurrent with zinc ion coordination. The H-bonds and zinc coordination in the four monomers varies very little. In the side-chain region of SAHA (suberoyl group), most interactions are hydrophobic and exhibit some degree of mobility. Interestingly, the ring moiety (amide-phenyl group) lacks interactions and shows marked mobility, as occurs with its nearby residues. These amino acids show that residues near the ring have greater mobility and those closer to the Zn-ion show invariability. **Figure 4** superimposes variations in the four SAHA molecules embedded in the catalytic core of the enzyme. The 11 adjacent residues and Zn-ion are included, as are dipole moment vectors.

3.4. Conformational Variability of SAHA Molecules and Residues of the Enzyme Binding Pocket

Comparison by superimposition of the four SAHA molecules shows important conformational variations near the phenyl group, but to a lesser extent near the suberoyl side-chain. The hydroxamic acid region is nearly invariable. Conformer B is the most distorted, followed by C, while conformers A and D have similar structures. Likewise, amino acids near the phenyl ring and contiguous suberoyl

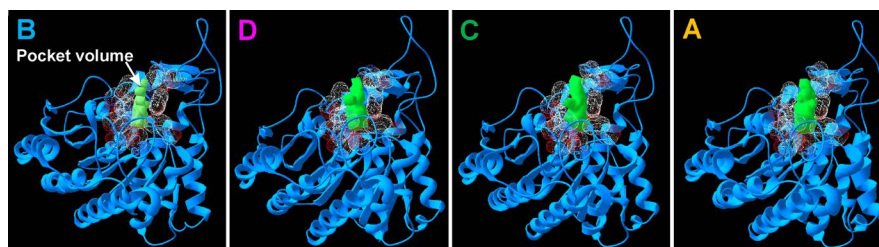
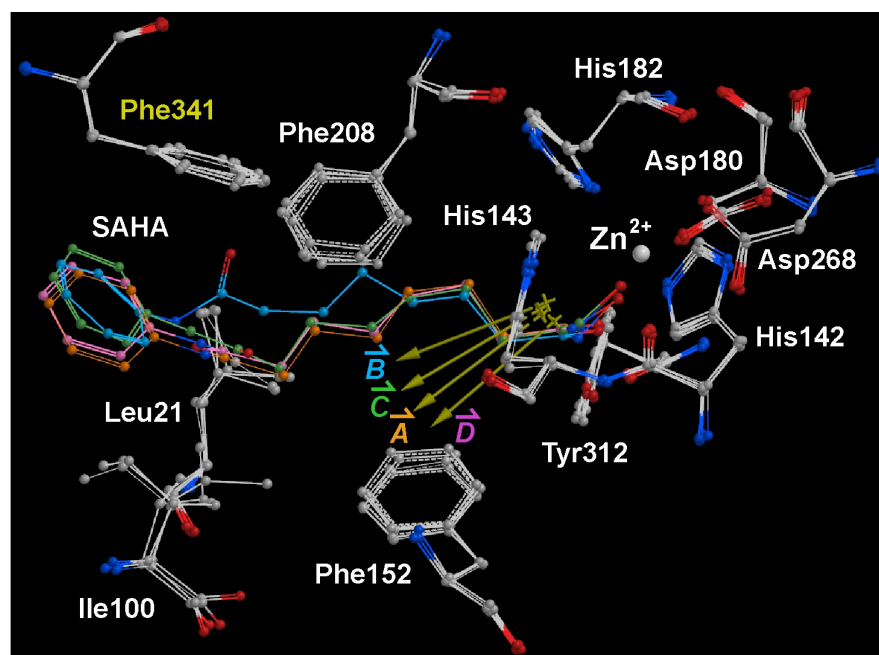
Table 3. RMSD values among the six pairs for the four SAHA monomers.

Monomer	RMSD (Å)	Monomer	RMSD (Å)
A and C	0.063	A and D	0.079
B and C	0.337	C and D	0.452
A and B	0.506	B and D	0.549

Table 4. Different monomer trends of the binding pocket volume and SAHA's area and volume values.

Monomer	Binding Pocket Volume (Å ³)*	Monomer	SAHA Area (Å ²)	Monomer	SAHA Volume (Å ³)**
B	116	B	180	D	280.86
D	153	C	223	A	281.11
C	166	A	230	B	281.35
A	189	D	249	C	281.40

*From lowest to highest values; **Trend with negligible differences.

**Figure 3.** Shape and position of the enzyme binding pocket (green). The binding pocket volume is arranged from smallest to the largest value among monomers. Surrounding residues are depicted in red.**Figure 4.** Overlapping of the enzyme-SAHA complex of the four monomers in the catalytic site from crystal PDB ID: 1ZZ1. SAHA is colored similar to the corresponding monomer; that is: A (orange), B (blue), C (green) and D (pink). Residues Ile100, Leu21, Phe152 and Phe208 are markedly closer to the SAHA-ring area and show larger conformational changes among monomers, while the hydroxamic group closer to the zinc ion, the polar residues: Tyr312, Asp180 and 268 and His142, 143 and 182 and Phe341 (yellow) from the adjacent asymmetric monomer remain almost invariable. The four Zn atoms overlay in the same place. Dipole moment vectors show similar tendencies.

chain have more conformational variability than those interacting with the hydroxamic acid moiety. **Figure 5** shows the conformation variability of SAHA and the 11 residues of the deacetylase catalytic pocket.

3.5. Amino Acids, Dihedral Angle Analysis

The conformational variability of residues (Aa) was assessed by measuring the dihedral angles of the 11 residues of each of the four monomer binding pockets. Thus, four residues: Leu21, Ile100, Phe208 and Tyr312 showed significant differences in χ_1 and χ_2 dihedral angles among the four monomers. Thus, the χ_2 and χ_1 dihedral angles of Ile100 and Phe341, respectively, were slightly rotated to correct atomic distances with SAHA.

Notably, the backbone ψ angle in Ile100 differed only in monomer B. The observed dihedral angle variations correlate quite well with the conformational differences observed in the overlapping of SAHA-enzyme complexes. **Table 5** shows the values of the measured dihedral angles; significant differences among monomers and their respective residues are highlighted.

3.6. Analysis of the Hydrophobic Interactions of SAHA-Enzyme Complexes in the Binding Pocket

The abundant and different hydrophobic interactions were analyzed both individually and collectively. Important hydrophobic interactions occur between the suberoyl backbone of SAHA and seven residues of the catalytic pocket. Three of them, Leu21, Ile100 and the aromatic Phe208, show among the four monomers a different number of interactions and different interacting atoms. Notably, Leu21 and Ile100 show the largest atomic distances variability. The other three residues which are aromatic, *i.e.*, Phe152, His182 and Tyr312, interact almost in the same

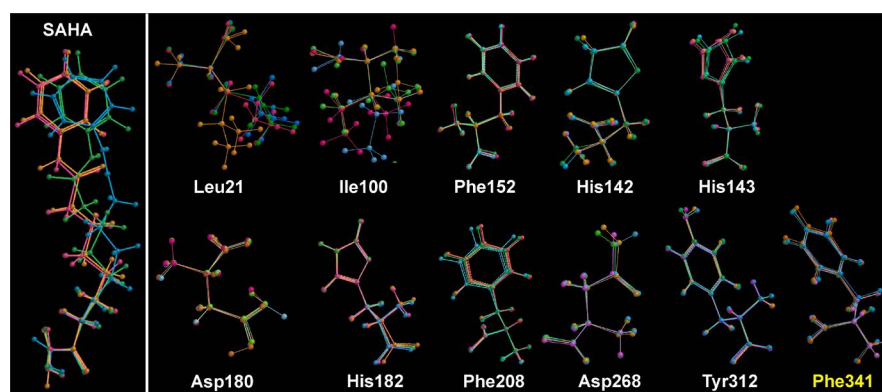


Figure 5. Conformation variability of SAHA and binding pocket residues. Monomers B and C (blue and green, respectively) fluctuated most. Mobility is larger at the phenyl ring followed by the suberoyl chain. The 11 neighbour amino acids forming the catalytic pocket of the enzyme are presented from the most variable Leu21 to the almost unvarying Tyr312 and Phe341 (yellow) from the adjacent asymmetric monomer. The five most variable residues are those close to the phenyl ring and suberoyl chain. The almost unchanged residues are those close to the hydroxamic acid and the Zn ion. Colors correspond to the respective monomer: A (orange), B (blue), C (green) and D (pink).

Table 5. Dihedral angles for each residue from catalytic site of monomers A, B, C and D.

Aa	Dihedral Angles																			
	Monomer A					Monomer B					Monomer C					Monomer D				
	Φ	Ψ	χ_1	χ_2	χ_3	Φ	Ψ	χ_1	χ_2	χ_3	Φ	Ψ	χ_1	χ_2	χ_3	Φ	Ψ	χ_1	χ_2	χ_3
Leu21	-155	-73	-142	-150		-153	-70	178	68		-151	-73	177	53		-156	-69	-171	65	
Ile100	-126	-36	-59	-60		-127	8	63	100*		-128	-48	-65	-72		-123	-34	173	148	
Phe208	-161	137	-165	81	-177	-166	136	-175	79	-177	-163	135	-172	-96	177	-162	134	-169	-97	177
Tyr312	-133	3	-56	-75	177	-135	5	-58	99	-176	-133	5	-57	-75	176	-135	3	-56	97	-176
His142	-70	-16	75	150	-180	-71	-13	74	154	180	-70	-16	71	155	-180	-68	-17	73	154	180
His143	-86	-17	-67	-51	-179	-88	-13	-61	-53	-178	-85	-16	-67	-49	-179	-83	-19	-69	-47	179
Asp268	-81	0	38	9		-80	1	39	8		-79	-1	37	11		-77	-6	40	8	
Phe152	80	-3	-46	149	180	79	-1	-43	146	179	78	1	-47	151	178	80	2	-47	152	179
Asp180	-52	143	174	-64		-52	143	177	-61		-50	142	177	-66		-52	140	178	-65	
His182	-102	156	-51	100	-180	-96	155	-57	106	-177	-98	154	-56	105	-177	-97	157	-55	102	-178
	Monomer D					Monomer C					Monomer B					Monomer A				
Phe341	-52	-47	177	62	179	-54	-42	169*	69	-180	-58	-45	174	64	178	-55	-45	174	67	180

Larger variations in dihedral angles are in boldface. *Ile100- χ_2 dihedral angle rotated from 160° to 100° in mB and Phe341- χ_1 dihedral angle rotated from 175° to 169° in the adjacent asymmetric monomer (mC). Dihedral angles and related atoms: Φ : C-N-C α -C. Ψ : N-C-C α -N. χ_1 : N-C α -C β -C γ (His, Leu, Phe, Tyr, Asp, Ile). χ_2 : C α -C β -C γ 1-C δ (Ile), C α -C β -C γ -C δ 1 (Leu, Phe, Tyr), C α -C β -C γ -O δ 1 (Asp), C α -C β -C γ -N δ 1 (His). χ_3 : C β -C γ -C δ 1-C ϵ 1 (Phe, Tyr), C β -C γ -N δ 1-C ϵ (His).

way through van der Waals forces between the aromatic ring of each one of them and the aliphatic chain of SAHA. Phe152 for instance, interacts similarly in monomers A and B, while, Tyr 312 interacts with monomers A and D and His182 presents two different type of interactions, one comprising A and D monomers and the other one including B and C monomers. Ile100 is the only non-polar residue that interacts with the amide phenyl group of SAHA. It is noteworthy that the SAHA amide-phenyl group is almost free of hydrophobic contacts showing high mobility, yielding different positions in the four monomers. Particularly, Phe341 the seventh residue from the adjacent asymmetric monomer showed two hydrophobic interactions in a similar manner in mA, mC and mD while in mB six interactions were observed. **Figure 6** shows the characteristic interactions of SAHA with the main six hydrophobic amino acids in the binding pocket of the four monomers from the FB188 HDAH crystal. Phe341 the seventh residue from the adjacent asymmetric monomer is not shown. Additionally, in **Table 6**, are shown Leu21 and Ile100 as an example of varied atomic interactions with SAHA in the four monomers.

Seven amino acids—five aromatic and two aliphatic—form the hydrophobic core that surrounds the SAHA molecule. However, a close view shows a different arrangement of hydrophobic interactions for the four monomers. Most hydrophobic interactions occur in the SAHA suberoyl backbone. The rings of the

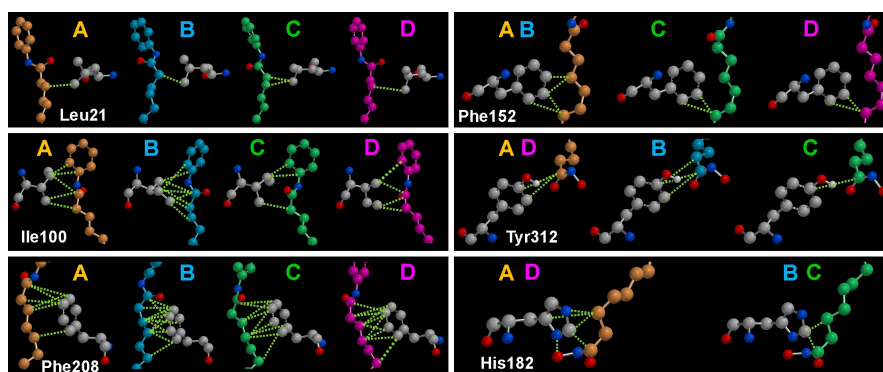


Figure 6. Characteristic hydrophobic interactions of six amino acids with SAHA in the four crystal monomers. The three amino acids with different type and number of contacts in the four monomers are shown in the left panel. In the right panel, Phe152 has a similar pattern of interactions with A and B monomers. Similarly, Tyr312 displays the same interactions with A and D monomers, while His182 has the same contacts with mA and mD, but a different pattern with B and C monomers. Phe341 from the adjacent asymmetric monomer not shown.

Table 6. Hydrophobic interactions for residues Leu21 and Ile100 with SAHA monomers.

Monomer	Residue	Number of Contacts	Interacting Atoms		
			Residue Atoms	SAHA Atom	Distance (Å)
A	Leu21	1	C δ 2	C6	4.0
			C γ 1	C8	3.8
	Ile100	5	C γ 1	C9	3.8
			C γ 2	C10	3.7
			C γ 2	C7	3.9
B	Leu21	1	C δ 1	C7	3.6
			Ile100	8	C δ 1
	C δ 1	C7			2.6* - 3.8
	C γ 1	C7	3.8		
	C γ 1	C8	4.0		
	C γ 1	C14	3.9		
	C γ 2	C8	4.0		
	C γ 2	C9	3.6		
C	Leu21	2	C δ 1	C6	3.9
			C δ 1	C7	4.0
	Ile100	3	C γ 1	C9	3.8
			C γ 1	C10	3.5* - 3.6
D	Leu21	1	C δ 1	C7	4.0
			Ile100	4	C δ 1
	C γ 1	C8			3.3* - 3.6
	C γ 2	C8			3.8
	C γ 2	C10	3.8		

Minimal interatomic distance allowed was 3.6 Å. *Abnormal shorter distances adjusted to 3.6 - 3.8 Å.

aromatic residues clearly interact to different extents among the four monomers. Thus, the A and D monomers have 24 and 26 interactions, respectively, while mC has the lower score with 20 and B has the highest, with 35 contacts. Ile100 and Phe341 are the only residues that interact with the SAHA ring. Ile100 interact with SAHA at two, one and one abnormal shortest distances in mB, mC and mD, respectively (all corrected to 3.6 Å before calculations). **Figure 7** shows the varying hydrophobic environments of the SAHA-enzyme catalytic binding pocket in the four monomers of the FB188 HDAH crystal.

3.7. Hydrogen Bonds

An invariable network of eight H-bonds occurs in the four monomers among the hydroxamic acid moiety of SAHA and the polar atoms of histidines 142, 143 and 182, aspartic acids 180 and 268 and Tyr312. The zinc ion is surrounded, to some extent, by the H-bond network. Unlike the hydrophobic interactions, the H-bonds are defined in a similar number and placement in the four monomers, creating a stable polar environment. **Figure 8** shows the H-bond network for the four monomers. A data summary of distances and H-bonding atoms is shown in **Table 7**.

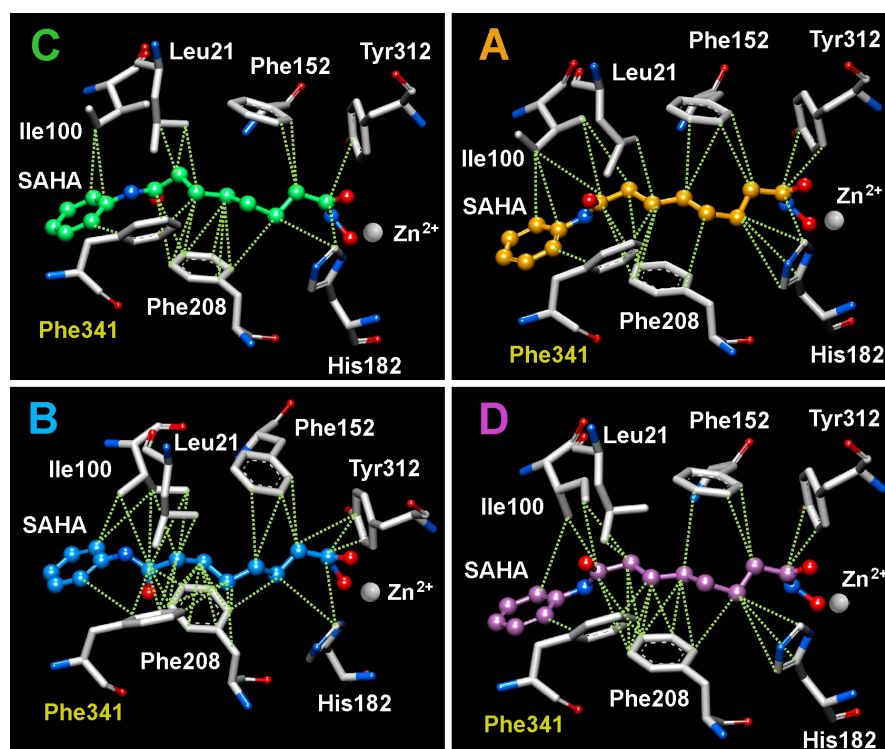


Figure 7. Hydrophobic interactions of SAHA and the residues of the catalytic pocket. Monomer C (shown first), has the fewest hydrophobic contacts, while the most contacts are found in monomer B. Although monomers A and D have similar hydrophobic interactions, their pattern of interaction is quite different. Leu21 and Ile100 present the largest conformational variations among the seven residues. Anomalous shorter distances of Ile100 are found in monomers B, C and D. The Zn ion is included for reference and SAHA molecules keep their assigned colors.

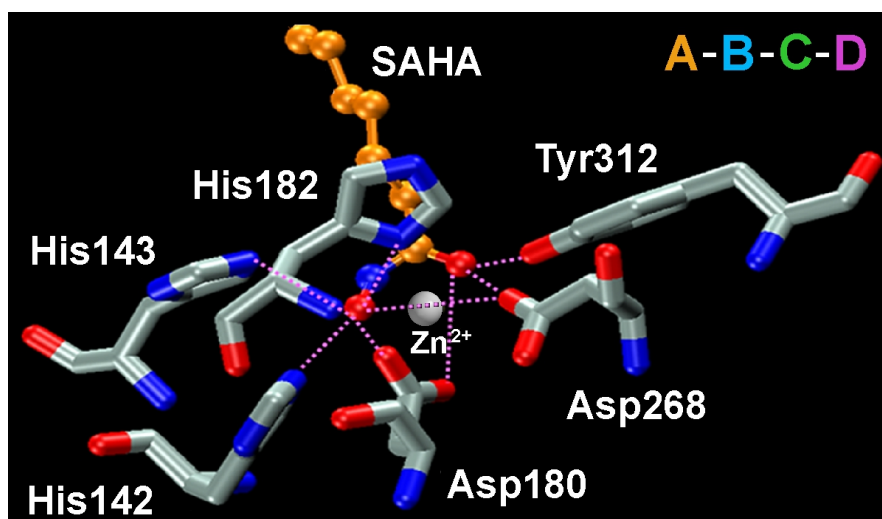


Figure 8. Close view of the H-bond network as observed in the four monomers of the enzyme-SAHA complexes. The H-bond network results from the negative oxygen charges from the hydroxamic acid of SAHA and the concurrent positive charges of the N-atoms of histidines 142, 143 and 182, the carbonyl and hydroxyl groups of aspartic acids 180 and 268, and the hydroxyl group of Tyr312. The symmetry of the H-bond network in the four monomers is remarkable and includes the nearby zinc ion in the same position.

Table 7. Hydrogen bond interactions from SAHA-residues complexes.

Monomer	Residue	H-bonds	Interacting Atoms		Distances (Å) A B C D
			Residue	SAHA	
A, B, C, D	His142	1	Nε2	O1	2.5, 2.5, 2.5, 2.4
	His143	1	Nε2	O1	3.0, 2.8, 3.1, 3.1
	Asp180	2	Oδ2	O1H	2.3, 2.1, 2.2, 2.4
			Oδ1H	O1	2.0, 2.1, 2.0, 2.3
	Asp268	2	Oδ2H	O2,	2.9, 2.7, 2.9, 2.8
				O1	4.0, 4.0, 4.0, 3.9
Tyr312	1	OH	O2	2.4, 2.4, 2.5, 2.6	
Total 7					

The Zn^{2+} coordination forms an octahedral-symmetrical bi-tetrahedral geometry in the four monomers. Two oxygen atoms of the hydroxamic acid of SAHA form two vertices, and the four that remain are shared with the oxygen atoms of Asp180 and Asp268 and the nitrogen atom of His182. The neat octahedral structure makes the zinc ion a strong center of union and stability for the enzyme-SAHA complex. **Figure 9** shows the coordination geometry of the complex formed by Zn^{2+} , SAHA and the three residues. **Table 8** shows data for coordinated atoms and their respective distances.

3.8. Sum of the SAHA-Catalytic Pocket Electrostatic Interactions

Each of the four monomers of SAHA clearly interacts with the catalytic pocket of the FB188 HDAH enzyme through 11 amino acids and one zinc ion. The

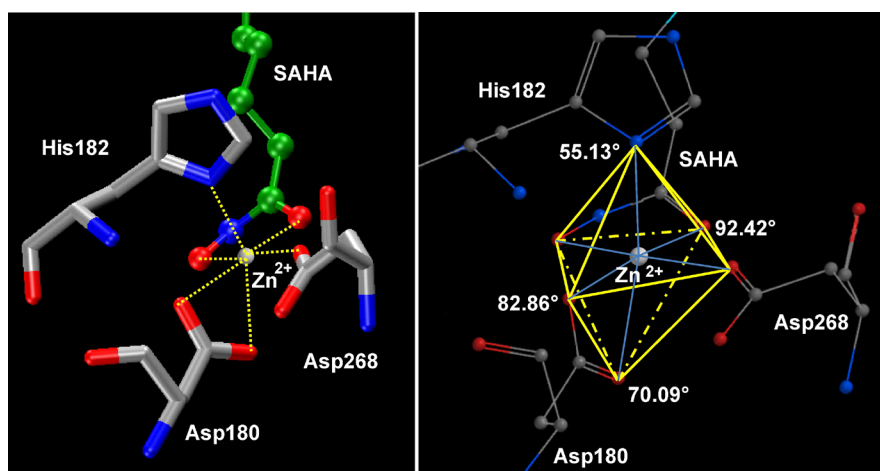


Figure 9. Zinc-ion forming an octahedral coordination with SAHA and adjacent polar atoms. The similarity of the coordination geometry of Zn^{2+} among the four monomers is remarkable. Two-ligand coordination is directed to the SAHA oxygen terminal atoms; two are shared with the two carboxyl oxygen atoms of Asp180, and the remaining two are directed to Asp268 and the N δ 1-atom of His182. The internal vertex angles are marked.

Table 8. Zinc interactions from SAHA-residues complexes.

Monomer	Residue	Number of Interactions	Residue Atoms	Distances (Å)			
				A	B	C	D
A, B, C, D	Asp180	2	O δ 2	2.0	2.0	2.1	2.0
			O δ 1	2.2	2.3	2.4	2.4
	His182	1	N δ 1	2.2	2.2	2.2	2.2
	Asp268	1	O δ 2	2.1	2.0	2.0	2.0
Total 4							

number of van der Waals contacts (hydrophobic interactions) varies from 20 to 35. However, eight hydrogen bonds and the Zn^{2+} octahedral shape coordination did not vary. **Table 9** shows all data for the SAHA-FB188 HDAH interactions and the range of their respective distances.

3.9. Electrostatic Properties

The extent of the electrostatic properties in the binding pocket of the SAHA-enzyme complex was evaluated by measuring the dipole moment, electrostatic potential and atomic charges of each monomer.

3.10. Dipole Moment Assessment

The dipole moment (DM) vector (Debyes), induced by the atomic charge arrangement, is the result of the SAHA-residues- Zn^{2+} interaction in the binding pocket of the four monomers and is oriented in almost the same direction toward Phe152 (see **Figure 4**). However, the DM magnitude of mA was shortest while the magnitude of mD was longest. The DM vector value, organized from the lowest to the highest was 12.4, 21.6, 28.2 and 37.3 for monomers A, D, C and B, respectively.

Table 9. Total interactions found among SAHA, amino acids and Zn²⁺ in the binding pocket of the four monomers of the crystal of the SAHA-FB188 HDAH complex.

Monomer	Aa	Hydrophobic interaction	Hydrophobic Distance*	H-bonds	H-bond Distance	Zn ²⁺ Interaction	Zn ²⁺ →SAHA Distance	Zn ²⁺ Aa interaction	Zn ²⁺ → Aa Distance
A	11	24	3.51 – 3.98	8	2.40 – 1.61	2	1.9 – 2.2	4	2.0 – 2.2
B	11	36	3.01 – 3.96	8	2.36 – 1.47	2	2.0 – 2.1	4	2.0 – 2.3
C	11	21	3.43 – 3.99	8	2.28 – 1.64	2	2.0 – 2.1	4	2.0 – 2.4
D	11	26	3.27 – 4.00	8	2.34 – 1.63	2	2.0 – 2.1	4	2.0 – 2.4

Zn²⁺→ Coordination distances; *Range-Distances in Å.

3.11. Molecular Electrostatic Potential in the SAHA-Binding Pocket Complex

The electrostatic potential maps of the binding pocket differed somewhat among the four monomers. As expected, the three molecular regions of SAHA have different patterns of MEPs, but showed almost the same pattern in the hydroxamic acid group and the Zn²⁺ ion in all cases. In contrast, the O and N atoms of the amide-phenyl group adopt different MEP patterns according to the orientation of those atoms in each monomer. A neutral and extended electronic region is observed along the suberoyl hydrophobic chain, highlighting the variable contour of the antagonist. The MEP map also shows matching of anionic and cationic groups in some residues, for instance, His142, Asp180, Asp268 and Tyr312 with the SAHA molecule, particularly in the hydroxamic acid group and the Zn²⁺-ion region. This interaction between SAHA and the enzyme shows important differences in the arrangement of binding site structures. The surfaces of the MEPs were set to an isodensity of 0.002 a.u. **Figure 10** shows a map view of the four SAHA-amino acid complexes.

3.12. Atomic Charge Calculations

The atomic charge values of SAHA and the involved atoms from residues that form the binding pocket were measured under bound and unbound conditions. Many atomic charges changed somewhat in the two conditions. Thus, the extent of charge modification in the interaction process was assessed by measuring differences in both conditions. An illustration of the atomic charge differences is shown in **Figure 11**.

3.13. Free Energy Analysis

After applying Equations (1) (2) and (3) (see methods), the free energy of each of the 11 residues was calculated individually, as were the free energies of SAHA and those of Zn²⁺-ion coordination in the four monomers. Clearly, conformational differences and the resulting electrostatic properties found in each of the four conformers are related to differences in free energy values. Interestingly, monomer B exhibited the largest differences in conformation and properties, including the highest free energy. Comprehensive data for each residue, Zn²⁺-ion

Table 10. Total binding free energies for FB188 HDAH monomers complexed with SAHA.

Monomer	Free energies for SAHA-residues and SAHA-Zn ²⁺ (kcal/mol)								Free energies for Zn ²⁺ -coordinated residues (kcal/mol)			Total free energies (kcal/mol)	
	Leu 21	Ile 100	His 142	His 143	Phe 152	Phe 208	Tyr 312	Phe 341	Zn ²⁺	Asp 180	His 182		Asp 268
B	-2.54	-2.08*	3.27	-4.18	-3.96	13.84	2.80	-2.81*	-114.90	-132.94	-165.90	-146.29	-555.69
C	-1.94	-4.56	1.77	-2.73	-5.87	-9.60	1.26	-3.55	-125.75	-131.33	-169.80	-146.19	-598.29
A	-3.41	-5.11	3.39	-9.42	-5.80	-9.18	2.38	-3.29	-161.68	-133.53	-168.12	-131.74	-625.51
D	-3.04	1.99	8.97	-5.06	-6.16	-8.81	-0.32	-2.78	-187.35	-131.14	-169.27	-145.19	-648.16

*Free energies after tuning the side chain angles of Ile100 and Phe341.

ring, the smallest binding pocket volume, the most hydrophobic contacts, the largest dipole moment and the highest total free energy. **Figure 12** shows the free energy trend for the four crystal monomers, comparing their experimental SAHA-enzyme inhibition.

4. Discussion

The X-ray crystal structures of these proteins have proven to be useful in studying properties beyond precise structure and electrostatic properties. The analysis of protein crystal structure using proper ligands or antagonists may contribute to the understanding of the mechanism of action of drugs, as reported for aspirin [21]. Another example is the demonstration of the conversion of rhodopsin to bathorhodopsin via a visual photochemical process, as reported by Nakamichi and Okada [22]. X-ray structures of HDACs have been used to design selective inhibitors [23] and to explore potential zinc binding groups to inhibit histone deacetylases [24]. In the present work, we studied the crystal of the histone deacetylase-like protein (FB188 HDAH) from a dynamic point of view; the protein is composed of four monomers that include the inhibitor SAHA in the binding pocket (PDB ID: 1ZZ1).

The underlying forces of the inhibitory mechanism of SAHA on FB188 HDAH were unveiled to a greater extent by systematic analysis of the PDB: 1ZZ1 crystal. The four monomers of the crystal varied in both structure and electronic properties. Notably, in agreement with data obtained by molecular dynamics calculations by Estiu *et al.* [25], SAHA varied mostly at the phenyl ring region yielding, differences in total energy and electrostatic properties. In contrast, the zinc region of the enzyme was quite stable. In addition, the four HDAH molecules showed variation in the binding pocket dimensions, along with conformational differences in SAHA and amino acids that form the binding pocket. Notably, the hydrogen bonds and Zn²⁺ SAHA-enzyme coordinated interactions were almost invariable, while the hydrophobic interactions changed considerably. The free energy changes among the four monomers resembling the typical pattern curve coincided with the pharmacological inhibition process.

Since the FB188 HDAH is a metalloenzyme that contains a zinc atom, it has six short coordination bonds (1.9 to 2.2 Å) that form an octahedral structure as

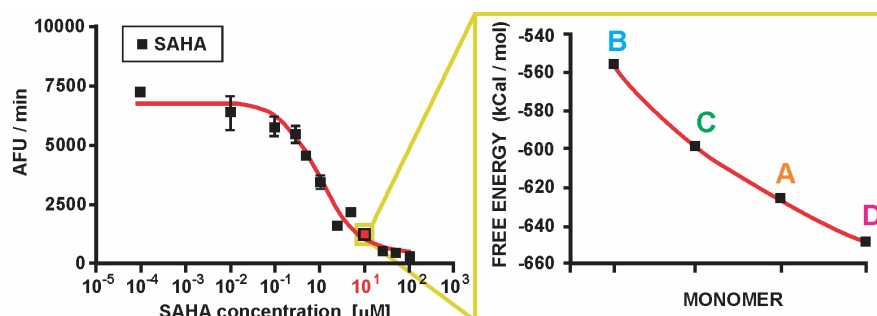


Figure 12. Comparison of the free-energy fitting curve of four monomers with the experimental curve of SAHA inhibition. On the right, an inset shows the present results of the SAHA enzyme-antagonism curve, unveiled theoretically by monomer analysis of the 1ZZ1 crystal. In addition a linear equation between B and D monomers gave a slope value of 0.81. On the left, comparison of the reported experimental curve of SAHA inhibition of FB188 HDAH [14].

reported by Nielsen *et al.* [15]. The zinc-ion produces markedly high stability of the complex, along with a network of eight H-bonds to SAHA, three histidines, two aspartic acids and one tyrosine. The zinc coordination and H-bond network are quite similar in the four monomers, suggesting that the SAHA-zinc interaction is the strongest and most stable in the SAHA-FB188 HDAH complex and is, therefore, the main inhibition site. In fact, the strain energy for the six zinc coordinations may stabilize the zinc-SAHA-H-bonds complex to improve SAHA efficacy as a time-independent antagonist with strong binding and low flexibility, as reported by Bressi *et al.* [26]. It has been suggested that changes in coordination strain can modify the electrostatic forces of the zinc ion and protein residues that form the coordinated complex. Likewise, zinc electrophilicity enhances the ability of zinc metalloenzymes to discriminate between reaction-coordinated species [27]. For example, some zinc metalloenzymes such as HDAC8 and thermolysin that may differ in the flexibility of their catalytic zinc coordination are capable of hydrolyzing the amide bond [28].

Indeed, the atomic arrangement in the catalytic site favors the entatic state, as suggested by Vallee and Williams [29]. This means that the enzyme is tense with the precise strain to proceed with the catalytic reaction, as supported by the preorganization theory of Warshel [30] whereby enzyme atomic networks are preorganized to react. These qualities in the enzyme environment may help to facilitate the antagonist effect of SAHA, particularly the interaction of the hydroxamic acid moiety. This group appears to be the real pharmacophore of SAHA and somewhat resembles the acetate group of acetyl-lysine, the natural substrate of histone deacetylases.

The binding pocket is an important factor for histone-deacetylase catalytic activity or inhibition. The volume of the binding pocket may vary, as observed in our calculations where its volume ranged from 116 to 189 Å³ among the monomers. In some cases, there is an adjacent 14-Å long cavity to the binding pocket [9], called the foot pocket [26], which may be or may be not filled by various inhibitors. In the case of SAHA, the binding pocket is occupied to maintain coor-

dination with the zinc ion. However, HDAC2 antagonists such as anilides may occupy the foot pocket and act as time-dependent inhibitors [26].

In addition, SAHA (the zinc chelator itself), is an interesting compound. According to Richon *et al.* [31], SAHA was synthesized to test the possibility that a hydrophobic phenyl group at one end of the molecule might enhance its activity. The crystal analysis of SAHA showed two positions for the phenyl group in the cap of SAHA, in agreement with the preferred orientation observed using molecular dynamics simulations [32]. In addition, the amide group is able to rotate, as observed in mB and mC. These conformational differences may explain variations in the inhibitory mechanism of SAHA. In fact, the SAHA in mB, the most dissimilar of the monomers, also had the largest differences in properties, including two anomalously short interatomic distances and the highest free energy. In addition, the SAHA molecule from mB had the highest energy and largest HOMO-LUMO gap, implying larger electron affinity, ionization potential and chemical hardness, among other properties. Although SAHA from mB had an acceptable conformation, its inhibitory activity was lowest. Pharmacologically, SAHA is a nanomolar inhibitor of HDAC activity [33]. However, the selectivity of SAHA appears to be low with respect to the human HDAC isoform classes and is classified as a non-selective inhibitor of class 1 and 2 enzymes [32]. Thus, SAHA acts as a broad-spectrum HDAC inhibitor [34] with different inhibitory potency depending on the HDAC class studied. Additionally, the inhibition of SAHA is not time-dependent [26]. Clinical trials have shown that SAHA is well tolerated; antitumor activity and the pharmacokinetic analysis showed that SAHA is rapidly eliminated in a manner proportional to the administered doses [35]. Notably, SAHA also inhibits esterase and lipase activities [36].

5. Conclusion

The tetrameric structure in the asymmetric unit cell of the crystal of the HDAC-like protein FB188 complexed with SAHA (PDB ID: 1ZZ1) proved a suitable model to disclose the biophysical mechanism of the SAHA enzyme inhibition process, which may contribute to our understanding of the epigenetic mechanism derived from histone modifications. By applying quantum mechanics and computational chemistry, in the systematic crystal analysis comprising the electronic structure, physicochemical properties and free energy calculations uncovered a dynamic process inside the crystal monomers. One invariable Zn²⁺ SAHA-enzyme coordinate interaction region and one highly variable amide-phenyl group region were clearly observed and were needed to slightly adjust some interatomic distances to validate the results. All conformational and physicochemical binding values varied among the four monomers that gave different free energy values for each monomer, showing a clear dynamic curve in typical inhibitory fashion. In this manner, it was demonstrated that the interior crystal structure gave sufficient information to unveil the free energy and biophysical mechanism of any bounded molecular system, using a quantum chemical analy-

sis of the various monomers present in a crystal.

References

- [1] Gregoret, I.V., Lee, Y.-M. and Goodson, H.V. (2004) Molecular Evolution of the Histone Deacetylase Family: Functional Implications of Phylogenetic Analysis. *Journal of Molecular Biology*, **338**, 17-31. <https://doi.org/10.1016/j.jmb.2004.02.006>
- [2] Marks, P.A., Miller, T. and Richon, V.M. (2003) Histone Deacetylases. *Current Opinion in Pharmacology*, **3**, 344-351. [https://doi.org/10.1016/S1471-4892\(03\)00084-5](https://doi.org/10.1016/S1471-4892(03)00084-5)
- [3] Kurdiani, S.K. and Grunstein, M. (2003) Histone Acetylation and Deacetylation in Yeast. *Nature Reviews Molecular Cell Biology*, **4**, 276-284. <https://doi.org/10.1038/nrm1075>
- [4] Hubbert, C., Guardiola, A., Shao, R., Kawaguchi, Y., Ito, A., Nixon, A., Yoshida, M., Wang, X.F. and Yao, T.P. (2002) HDAC6 Is a Microtubule-Associated Deacetylase. *Nature*, **417**, 455-458. <https://doi.org/10.1038/417455a>
- [5] Jones, P. and Baylin, S.B. (2002) The Fundamental Role of Epigenetic Events in Cancer. *Nature Reviews Genetics*, **3**, 415-428. <https://doi.org/10.1038/nrg816>
- [6] Govindarajan, N., Agis-Balboa, R.C., Walter, J., Sananbenesi, F. and Fischer, A. (2011) Sodium Butyrate Improves Memory Function in an Alzheimer's Disease Mouse Model When Administered at an Advanced Stage of Disease Progression. *Journal of Alzheimer's Disease*, **26**, 187-197. <https://doi.org/10.3233/JAD-2011-110080>
- [7] Sharma, R.P., Grayson, D.R. and Gavin, D.P. (2008) Histone Deacetylase 1 Expression Is Increased in the Prefrontal Cortex of Schizophrenia Subjects: Analysis of the National Brain Databank Microarray Collection. *Schizophrenia Research*, **98**, 111-117. <https://doi.org/10.1016/j.schres.2007.09.020>
- [8] Pons, D., de Vries, F.R., van den Elsen, P.J., Heijmans, B.T., Quax, P.H.A. and Jukema, J.W. (2009) Epigenetic Histone Acetylation Modifiers in Vascular Remodeling: New Targets for Therapy in Cardiovascular Disease. *European Heart Journal*, **30**, 266-277. <https://doi.org/10.1093/eurheartj/ehn603>
- [9] Finnin, M.S., Donigian, J.R., Cohen, A., Richon, V.M., Rifkind, R.A., Marks, P.A., Breslow, R. and Pavletich, N.P. (1999) Structures of a Histone Deacetylase Homologue Bound to the TSA and SAHA Inhibitors. *Nature*, **401**, 188-193. <https://doi.org/10.1038/43710>
- [10] Schuetz, A., Min, J., Allali-Hassani, A., Schapira, M., Shuen, M., Loppnau, P., Mazitschek, P.R., Kwiatkowski, N.P., Lewis, T.A., Maglathin, R.L., McLean, T.H., Bochkarev, A., Plotnikov, A.N., Vedadi, M. and Arrowsmith, C.H. (2008) Human HDAC7 Harbors a Class IIa Histone Deacetylase-Specific Zinc Binding Motif and Cryptic Deacetylase Activity. *Journal of Biological Chemistry*, **283**, 11355-11363. <https://doi.org/10.1074/jbc.M707362200>
- [11] Somoza, J.R., Skene, R.J., Katz, B.A., Mol, C., Ho, J.D., Jennings, A.J., Luong, C., Arvai, A., Buggy, J.J., Chi, E., Tang, J., Sang, B.C., Verner, E., Wynands, R., Leahy, E.M., Dougan, D.R., Snell, G., Navre, M., Knuth, M.W., Swanson, R.V., McRee, D.E. and Tari, L.W. (2004) Structural Snapshots of Human HDAC8 Provide Insights Into the Class I Histone Deacetylases. *Structure (Cambridge)*, **12**, 1325-1334. <https://doi.org/10.1016/j.str.2004.04.012>
- [12] Lauffer, B.E., Mintzer, R., Fong, R., Mukund, S., Tam, C., Zilberleyb, I., Flicke, I.B., Ritscher, A., Fedorowicz, G., Vallerio, R., Ortwine, D.F., Gunzner, J., Modrusan, Z.,

- Neumann, L., Koth, C.M., Lupardus, P.J., Kaminker, J.S., Heise, C.E. and Steiner, P. (2013) Histone Deacetylase (HDAC) Inhibitor Kinetic Rate Constants Correlate with Cellular Histone Acetylation but not Transcription and Cell Viability. *Journal of Biological Chemistry*, **288**, 26926-26943. <https://doi.org/10.1074/jbc.M113.490706>
- [13] Xu, W.S., Parmigiani, R.B. and Marks, P.A. (2006) Histone Deacetylase Inhibitors: Molecular Mechanisms of Action. *Oncogene*, **26**, 5541-5552. <https://doi.org/10.1038/sj.onc.1210620>
- [14] Hildmann, C., Ninkovic, M., Dietrich, R., Wegener, D., Riester, D., Zimmermann, D.T., Birch, O.M., Bernegger, C., Loidl, P. and Schwienhorst, A. (2004) A New Amidohydrolase from *Bordetella* or *Alcaligenes* Strain FB188 with Similarities to Histone Deacetylases. *Journal of Bacteriology*, **8**, 2328-2339. <https://doi.org/10.1128/JB.186.8.2328-2339.2004>
- [15] Nielsen, T.K., Hildmann, C., Dickmanns, A., Schwienhorst, A. and Ficner, R. (2005) Crystal Structure of a Bacterial Class 2 Histone Deacetylase Homologue. *Journal of Molecular Biology*, **354**, 107-120. <https://doi.org/10.1016/j.jmb.2005.09.065>
- [16] Bernstein, F.C., Koetzle, T.F., Williams, G.J., Meyer, E.E., Brice, M.D., Rodgers, J.R., Kennard, O., Shimanouchi, T. and Tasumi, M. (1997) The Protein Data Bank. *Journal of Molecular Biology*, **112**, 535-542. [https://doi.org/10.1016/S0022-2836\(77\)80200-3](https://doi.org/10.1016/S0022-2836(77)80200-3)
- [17] Humphrey, W., Dalke, A. and Schulten, K. (1996) VMD-Visual Molecular Dynamics. *Journal of Molecular Graphics*, **14**, 33-38. [https://doi.org/10.1016/0263-7855\(96\)00018-5](https://doi.org/10.1016/0263-7855(96)00018-5)
- [18] Moreland, J.L., Gramada, A., Buzko, O.V., Zhang, Q. and Bourne, P.E. (2005) The Molecular Biology Toolkit (MBT): A Modular Platform for Developing Molecular Visualization Applications. *BMC Bioinformatics*, **6**, 21. <https://doi.org/10.1186/1471-2105-6-21>
- [19] Guex, N. and Peitsch, M.C. (1997) Swiss-Model and the Swiss-PdbViewer: An Environment for Comparative Protein Modeling. *Electrophoresis*, **18**, 2714-2723. <https://doi.org/10.1002/elps.1150181505>
- [20] Spartan'14 (2014) Wavefunction Inc., Irvine.
- [21] Loll, P.J., Picot, D. and Garavito, R.M. (1995) Crystal Structure of a Bacterial Class 2 Histone Deacetylase Homologue. *Nature Structure and Biology*, **2**, 637-643. <https://doi.org/10.1038/nsb0895-637>
- [22] Nakamichi, H. and Okada, T. (2006) Crystallographic Analysis of Primary Visual Photochemistry. *Angewandte Chemie International Edition*, **45**, 4270-4273. <https://doi.org/10.1002/anie.200600595>
- [23] Wang, D.F., Helquist, P., Wiech, N.L. and Wiest, O. (2005) Toward Selective Histone Deacetylase Inhibitor Design: Homology Modeling, Docking Studies, and Molecular Dynamics Simulations of Human Class I Histone Deacetylases. *Journal of Medicinal Chemistry*, **48**, 6936-6947. <https://doi.org/10.1021/jm0505011>
- [24] Chen, K., Xu, L. and Wiest, O. (2013) Computational Exploration of Zinc Binding Groups for HDAC Inhibition. *Journal of Organic Chemistry*, **78**, 5051-5055. <https://doi.org/10.1021/jo400406g>
- [25] Estiu, G., Greenberg, E., Harrison, C.B., Kwiatkowski, N.P., Mazitschek, R.R., Bradner, J.E. and Wiest, O. (2008) Structural Origin of Selectivity in Class II-Selective Histone Deacetylase Inhibitors. *Journal of Medicinal Chemistry*, **51**, 2898-2906. <https://doi.org/10.1021/jm7015254>

- [26] Bressi, J.C., Jennings, A.J., Skene, R., Wu, Y., Melkus, R., De Jong R., O'Connell, R.S., Grimshaw, C.E., Navre, M. and Gangloff, A.R. (2010) Exploration of the HDAC2 Foot Pocket: Synthesis and SAR of Substituted N-(2-aminophenyl) Benzamides. *Bioorganic and Medicinal Chemistry Letters*, **20**, 3142-3145. <https://doi.org/10.1016/j.bmcl.2010.03.091>
- [27] Ataie, N.J., Hoang, Q.Q., Zahniser, M.P.D., Tu, Y., Milne, A., Petsko, G.A. and Ringe, D. (2008) Zinc Coordination Geometry and Ligand Binding Affinity: The structural and Kinetic Analysis of the Second-Shell Serine 228 Residue and the Methionine 180 Residue of the Aminopeptidase from *Vibrio proteolyticus*. *Biochemistry*, **47**, 7673-7683. <https://doi.org/10.1021/bi702188e>
- [28] Wu, R., Hu, P., Wang, S., Cao, Z. and Zhang, Y. (2010) Flexibility of Catalytic Zinc Coordination in Thermolysin and HDAC8: A Born-Oppenheimer *Ab Initio* QM/MM Molecular Dynamics Study. *Journal of Chemical Theory and Computational*, **6**, 337. <https://doi.org/10.1021/ct9005322>
- [29] Vallee, B.L. and Williams, R.J.P. (1968) Metalloenzymes: The Entatic Nature of Their Active Sites. *Proceedings of the National Academy of Sciences of the USA*, **59**, 498-505. <https://doi.org/10.1073/pnas.59.2.498>
- [30] Warshel, A. (1998) Electrostatic Origin of the Catalytic Power of Preorganized Active Sites. *Journal of Biological Chemistry*, **273**, 27035-27038. <https://doi.org/10.1074/jbc.273.42.27035>
- [31] Richon, V.M., Emiliani, S., Verdin, E., Webb, Y., Breslow, R., Rifkind, R.A. and Marks, P.A. (1998) A Class of Hybrid Polar Inducers of Transformed Cell Differentiation Inhibits Histone Deacetylases. *Proceedings of the National Academy of Sciences of the USA*, **95**, 3003-3007. <https://doi.org/10.1073/pnas.95.6.3003>
- [32] Estiu, G., West, N., Mazitschek, R.R., Greenberg, E., Bradner, J.E. and Wiest, O. (2010) On the Inhibition of Histone Deacetylase 8. *Bioorganic and Medicinal Chemistry*, **18**, 4103-4110. <https://doi.org/10.1016/j.bmc.2010.03.080>
- [33] Richon, V.M. (2006) Cancer Biology: Mechanism of Antitumour Action of Vorinostat (Suberoylanilide Hydroxamic Acid), a Novel Histone Deacetylase Inhibitor. *British Journal Cancer*, **95**, S2. <https://doi.org/10.1038/sj.bjc.6603463>
- [34] Methot, J.L., Chakravarty, P.K., Chenard, M., Close, J., Cruz, J.C., Dahlberg, W.K., Fleming, J., Hamblett, C.L., Hamill, J.E., Harrington, P., Harsch, A., Heidebrecht, R., Hughes, B., Jung, J., Kenific, C.M., Kral, A.M., Meinke, P.T., Middleton, R.E., Ozerova, N., Sloman, D.L., Stanton, M.G., Szewczak, A.A., Tyagarajan, S., Witter, D.J., Secrist, J.P. and Miller, T.A. (2008) Exploration of the Internal Cavity of Histone Deacetylase (HDAC) with Selective HDAC1/HDAC2 Inhibitors (SHI-1:2). *Bioorganic and Medicinal Chemistry Letters*, **18**, 973-978. <https://doi.org/10.1016/j.bmcl.2007.12.031>
- [35] Kelly, W.K., Richon, V.M., O'Connor, O., Curley, T., MacGregor-Curtelli, B., Tong, W., Klang, M., Schwartz, L., Richardson, S., Rosa, E., Drobnjak, M., Cordon-Cordo, C., Chiao, J.H., Rifkind, R., Marks, P.A. and Scher, H. (2003) Phase I Clinical Trial of Histone Deacetylase Inhibitor: Suberoylanilide Hydroxamic Acid Administered Intravenously. *Clinical Cancer Research*, **9**, 3578-3588.
- [36] Moreth, K., Riester, D., Hildmann, C., Hempel, R., Wegener, D., Schober, A. and Schwienhorst, A. (2007) An Active Site Tyrosine Residue Is Essential for Amidohydrolase but not for Esterase Activity of a Class 2 Histone Deacetylase-Like Bacterial Enzyme. *Biochemical Journal*, **401**, 659-665. <https://doi.org/10.1042/BJ20061239>

Abbreviations

FB188 HDAH: HDAC-like amidohydrolase, histone deacetylase-like protein;
HAT: histone acetyltransferases;
HDAC: histone deacetylase;
SAHA: suberoylanilide hydroxamic acid;
DFT: Density Functional Theory;
PDB: Protein Data Bank;
TSA: trichostatin A;
NAD: nicotinamide adenine dinucleotide;
mA, mB, mC, and mD; monomers named A, B, C and D respectively;
RMSD: root-mean-square deviation;
MEP: molecular electrostatic potential;
Aa: residues;
B-factor: thermal-factor;
 χ_1 : dihedral angle N-C α -C β -C γ ;
 χ_2 : dihedral angle C α -C β -C γ -C δ ;
DM: dipole moment.